Journal of Materials Chemistry C

ROYAL SOCIETY OF CHEMISTRY

PAPER

View Article Online
View Journal | View Issue



Cite this: J. Mater. Chem. C, 2021, 9, 12342

# Highly efficient and thermally robust cyan-green phosphor-in-glass films for high-brightness laser lighting†

Huajun Wu, [a] Guo-Hui Pan, [a] Zhendong Hao, *[a] Liangliang Zhang, [a] Hao Wu [a] and Jiahua Zhang *[ab]

Received 3rd June 2021,
Accepted 22nd July 2021

DOI: 10.1039/d1tc02551a

rsc.li/materials-c

Laser-driven white lighting has drawn great attention due to its high-brightness, high efficiency and compact size. However, the current laser lighting usually suffers from a low color rendering ($R_a$ ~ 60) due to the presence of a wide "Cyan cavity" (460–530 nm) in the luminescence spectrum. Herein, we report on the preparation and characterization of a novel cyan-green color converter, namely $Ca_3Sc_2Si_3O_{12}:Ce^{3+},Na^+$ phosphor-in-glass (CSS-PiG) film. The addition of $Na^+$ as a charge compensator greatly improved the internal quantum efficiency (IQE) of CSS:$Ce^{3+}$ phosphors. Because of the good chemical stability and the matching refractive index between the glass matrix and embedded phosphors, the as-prepared CSS-PiG film exhibits an efficient cyan-green emission (with a peak at 508 nm and IQE ~91%) and excellent thermal stability (maintaining 75% of the room-temperature emission intensity at 300 °C). Under the excitation of a 14.5 W $mm^{-2}$ blue laser, the PiG film could produce a high-brightness white light with a forward luminous flux of 701 lm, a forward luminous efficacy of 112 lm $W^{-1}$ and a $R_a$ of 61. By coating a red-emitting $CaAlSiN_3:Eu^{2+}$ layer on the CSS-PiG film, the composite CSS-PiG/$CaAlSiN_3$ film shows an ultra-broadband emission with a full-width at half maximum (FWHM) of 196 nm, which remarkably narrows the "Cyan cavity" and thus provides a $R_a$ above 90. These results demonstrate that the CSS-PiG film is a promising candidate for laser lighting.

## 1. Introduction

Since the invention of gallium nitride (GaN)-based light emitting diodes (LEDs) in the early 1990s, white LEDs have attracted much attention due to their superior features, such as high efficiency, long life time and environmental friendliness.[1–4] Commercial white LEDs generate white light through a combination of blue GaN chips with various phosphors dispersed in organic silicone resin (phosphor in silicone, PiS).[5–9] However, the quantum efficiency (QE) of blue LED chips decreases at high input current density, which does not favor the achievement of high-efficiency and high-brightness devices using a single LED. In contrast to the LED chips, laser diodes (LD), free of the "Efficiency droop" effect and featuring controllable shaping and focusing of laser beams, are being considered as a novel excitation source for high-brightness white lighting.[10] Phosphor-converted white laser lighting based on blue LD activated remote phosphor systems promises cost effectiveness and high brightness, and is now dominating the market. The traditional organic PiS materials, however, suffer from low thermal conductivity and poor thermal stability, and would be damaged or burned under high-density laser irradiation.

As such, several all-inorganic color converters such as single crystals, phosphor ceramics, phosphor in glass (PiG) and phosphor films have been widely investigated for use in laser lighting.[11–13] Single crystals usually have excellent thermal ability and high internal quantum efficiency (IQE) owing to the perfect crystal structure, but they commonly have a low light absorption efficiency (AE) and poor light uniformity owing to the absence of light-scattering centers.[14,15] Phosphor ceramics are superior to single crystals because they offer a great tunability of microstructure to enhance the light scattering.[16–20] However, the fabrication of phosphor ceramics is complicated and costly, and most nitride phosphors are hard to be sintered into dense ceramics with acceptable optical properties. In contrast, PiG shows competitive advantages in terms of easy fabrication and great versatility of various phosphors, but its application in laser lighting is limited

[a] State Key Laboratory of Luminescence and Applications, Changchun Institute of Optics, Fine Mechanics and Physics, Chinese Academy of Sciences, 3888 Eastern South Lake Road, Changchun, 130033, China. E-mail: haozd@ciomp.ac.cn; Fax: +86-431-8617-6317

[b] Center of Materials Science and Optoelectronics Engineering, University of Chinese Academy of Sciences, Beijing, 100049, China. E-mail: zhangjh@ciomp.ac.cn

† Electronic supplementary information (ESI) available. See DOI: 10.1039/d1tc02551a

due to the low endurable laser power density ($\sim$1 W mm$^{-2}$) and poor thermal conductivity ($\sim$1 Wm$^{-1}$ K$^{-1}$).[21–24] An alternative solution to such problem was the design of the phosphor–substrate configuration, where a PiG film was coated on a substrate with high thermal conductivity.[25–30] Zheng *et al.* prepared a YAG-PiG film on a sapphire substrate. The film could endure a laser power density of 11.2 W mm$^{-2}$ and produce laser-driven white lighting with a luminous flux of 1839 lm and a Color Rendering Index ($R_a$) of 63.[30] Li *et al.* prepared a yellow-emitting $La_3Si_6N_{11}$:Ce-PiG film and the film gave an output of 1071 lm with a $R_a$ of 70.[26] Xu *et al.* successfully fabricated the red-emitting $CaAlSiN_3$:Ce-PiG film to improve the $R_a$ value.[27] Presently most of the color converters are based on yellow/red phosphor materials and the consequent color rendering of laser lighting remains low ($\sim$60). As for laser lighting, blue LD chips emit a narrow line-width blue laser with a full-width at half maximum (FWHM) of $\sim$2 nm, while blue LED chips emit a broad-band blue light with a FWHM of 20–40 nm. There always exists a wider "Cyan cavity" (460–530 nm) in the emission spectrum of phosphor-converted white laser lighting. However, much attention has been paid to the red and yellow inorganic color converters and only a few studies have focused on green-yellow converters such as LuAG:Ce PiG (peaking at 530 nm) or β-Sialon:Eu PiG film (peaking at 540 nm).[31–33] In addition, all of these color converters show weak cyan emission and could not fill the "Cyan cavity" effectively. Hence, the development of color converters with intense broadband cyan-green emission is in demand to improve the optical performance of laser lighting.

The cubic silicate garnet $Ca_3Sc_2Si_3O_{12}$:$Ce^{3+}$ (CSS:$Ce^{3+}$) has drawn much attention for LED lighting because of its compelling optical performance.[34,35] First, it has more blue-shifted emission spectrum (peaking at 505 nm) with a wide bandwidth, making it a promising candidate to fill the "Cyan cavity" and yield white light with a relatively high color rendering ($R_a \geq 85$). Second, the small Stokes shift helps to reduce the heat generation during the color down-conversion processes. Third, CSS:$Ce^{3+}$ phosphors have excellent chemical and thermal stability. At 600 K, the PL intensity only drops to 60% of the PL intensity at 80 K, while the PL intensity of the famous YAG:Ce phosphors drops to 30%.[36] These fascinating properties make CSS:$Ce^{3+}$ a promising phosphor for laser lighting. However, to the best our knowledge, the performance of CSS:$Ce^{3+}$ for laser lighting has never been studied. It is thus of great interest to investigate the optical performance of CSS:$Ce^{3+}$ under laser excitation and to develop its application in laser-driven solid state lighting.

In this work, pure CSS:$Ce^{3+}$,$Na^+$ phosphors, which possess high quantum efficiency and high thermal stability, were prepared by introducing charge compensatory additives $Na^+$. The low-melting-temperature borosilicate glass matrices with a similar refractive index to that of CSS:$Ce^{3+}$,$Na^+$ phosphors were carefully chosen as the inorganic binder. CSS-PiG films were then developed by cofiring the CSS:$Ce^{3+}$,$Na^+$ phosphors and glass powders on thermally conductive sapphire substrates. The sintering process, phosphor content and thickness of the PiG film were optimized for high luminescence efficiency. The optical performance of the film in laser lighting was systematically investigated. All the results demonstrate that our CSS-PiG film is a promising candidate for high-quality laser lighting.

## 2. Experimental section

### 2.1 Materials

High-purity $CaCO_3$ (Aladdin, China, 99.99%), $Sc_2O_3$ (Aladdin, China, 99.99%), $SiO_2$ (Aladdin, China, 99.99%), $NaHCO_3$ (Aladdin, China, 99.99%) and $CeO_2$ (Aladdin, China, 99.99%) are commercially available. Terpilenol (Aladdin, China, 98%) and ethyl cellulose (Aladdin, China, 99%) were used as the organic solvent and organic binder, respectively. The sapphire substrates with a size of 20 × 20 × 0.4 mm$^3$ were bought from Jiangsu Jeshine New Material Co. Ltd (China). Two silicone gels (SLC-3502, A, B) were bought from Chengdu Silicone Technology Co. Ltd (China).

### 2.2 Fabrication of phosphors and PiG films

**2.2.1 Fabrication of CSS:$Ce^{3+}$,$Na^+$ phosphors.** Phosphors with the general formula $(Ca_{2.88}Na_{0.06}Ce_{0.06})Sc_2Si_3O_{12}$ (CSS:$Ce^{3+}$,$Na^+$) were prepared by a solid state reaction method. The raw materials of high-purity $CaCO_3$, $Sc_2O_3$, $SiO_2$, $NaHCO_3$ and $CeO_2$ were weighed accurately according to stoichiometric proportions and thoroughly blended in an agate mortar for 30 min. The mixed powders were placed in an alumina crucible and then sintered in a tube furnace under a reducing atmosphere (95%$N_2$/5%$H_2$) at 1360 °C for 6 h. The resulting powders were finely ground for further characterization.

**2.2.2 Fabrication of PiG films.** To evaluate the optical performance of CSS:$Ce^{3+}$,$Na^+$ phosphors under high-power laser excitation, the PiG films were fabricated by cofiring the CSS:$Ce^{3+}$,$Na^+$ phosphors and glass powders. Low-temperature glass powders with the composition $26B_2O_3$-35ZnO-$12SiO_2$-$10La_2O_3$-$11WO_3$-$6Li_2O$ (in mol%) were prepared by using the conventional melting-quenching technique. Firstly, 3 wt% ethyl cellulose was dissolved in terpilenol by stirring with an agitator at 80 °C for 2 h to prepare the organic solvent. Then the CSS:$Ce^{3+}$,$Na^+$ phosphors, glass powders and organic solvent were added into an agate mortar and thoroughly mixed. The weight ratio of phosphors to glass powders (abbreviated as PiG ratio) was designed to be 1 : 4, 2 : 3, 3 : 2, and 4 : 1 (P1G4, P2G3, P3G2, P4G1). Afterwards, the resultant slurries were coated on the sapphire substrates by blade coating. The film thickness was controlled by the stack number of the tapes. Finally, the dried samples were sintered in a muffle furnace at different temperatures (600, 620, 640, 660 and 680 °C) and holding times (10, 20, 40 and 60 min) to optimize the sintering process.

To improve the color rendering, the red $CAlSiN_3$:$Eu^{2+}$ layers were coated on the PiG film. Firstly, the two silicone gel components A and B were mixed together at a mass ratio of 4 : 1. Subsequently, 7 wt% $CAlSiN_3$:$Eu^{2+}$ phosphors were added to the mixed gels and stirred thoroughly for 30 min. Then the obtained slurry was vacuumized at 0.01 MPa for 10 min to release the produced air bubbles. Finally, the red phosphor-in-silicone (PiS) paste was printed on the sintered-PiG film by

blade casting and then cured at 150 °C for 3 h in a drying oven. The thickness of the red PiS film was ~70 μm.

### 2.3 Characterization

The X-ray diffraction (XRD) patterns were collected by using a powder X-ray diffractometer (D8 Advance, Bruker, Germany) with Cu Kα radiation at 40 kV and 30 mA. The micrograph and elemental mappings of the samples were observed by using a scanning electron microscope (SEM, Model S-4800, Hitachi, Japan) equipped with an energy dispersive X-ray spectroscope (EDS). The photoluminescence (PL) and photoluminescence excitation (PLE) spectra were obtained by using a spectrometer equipped with a 150 W Xenon lamp (F-7000, Hitachi, Japan). The temperature-dependent PL spectra were recorded by using a home-made measurement system, which consisted of a 452 nm blue LD, a fluorescence microscope (BX53M, Olympus, Japan), a cooling/heating stage (THMS-600, Linkam, UK) and a charge-coupled device (CCD) spectrometer (QEPro, Ocean Optics, China). The samples were heated from 25 to 300 °C with a step size of 25 °C at a heating rate of 25 °C $min^{-1}$ and held for 1 min at each temperature. The total transmittance spectra of the samples were measured on a dual beam spectrophotometer (UV-3600 plus, Shimadzu, Japan) equipped with an integrating sphere. The electroluminescence (EL) properties of the samples under laser irradiation were measured by using an integrated test system (EVERFINE, China) including a photoelectric characteristic testing system, a rotating integral ball, a 452 nm LD and a high precision fast spectral radiometer (HAAS-2000). The optical power of the blue LD, as determined by the input current, was measured with a laser power meter (PM100D, THORLABS, USA). The laser spot was captured by using a beam analyzer (BC106N-VIS, THORLABS, USA) and the beam diameter was determined according to the International Organization for Standardization (ISO) 11146. The surface temperature of the samples was measured by using an infrared thermal imaging system (ETS320, FLIR, USA). The external quantum efficiency (EQE), IQE and AE values were measured under 445 nm excitation using an absolute photoluminescence quantum yield measurement system (Quantaurus-QY Plus C13534-12, Hamamatsu Photonics, Japan). All the measurements were conducted at room temperature unless otherwise stated.

## 3. Results and discussion

### 3.1 Properties of CSS:$Ce^{3+}$,$Na^{+}$ phosphors

The CSS host has a cubic Garnet-type structure with the *Ia3d* space group (No. 230).[37,38] In the structure, each $Ca^{2+}$ is surrounded by eight $O^{2-}$ ions to form a distorted dodecahedron. One $Sc^{3+}$ ion and six $O^{2-}$ ions constitute an octahedron, while $Si^{4+}$ and $O^{2-}$ ions constitute a tetrahedron. The synthesis of phase-pure CSS:$Ce^{3+}$ phosphors by solid-state methods

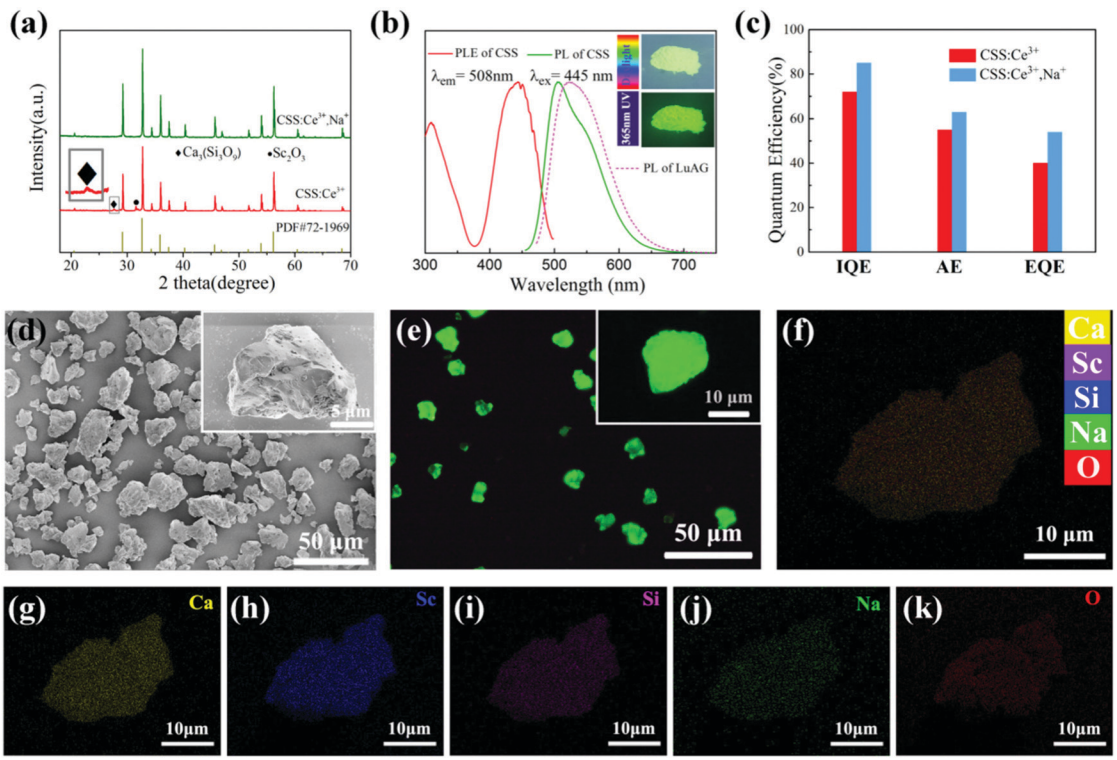


Fig. 1 (a) XRD patterns of the phosphors with and without $Na^{+}$ addition; (b) PL and PLE spectra of CSS:$Ce^{3+}$,$Na^{+}$ phosphors, and PL spectrum of LuAG:$Ce^{3+}$ phosphors; the inset is photographs of the CSS:$Ce^{3+}$,$Na^{+}$ phosphors under daylight and 365 nm UV light; (c) AE, IQE and EQE of phosphors with and without $Na^{+}$ addition under 445 nm excitation; (d) SEM image and (e) fluorescence microscope photograph of CSS:$Ce^{3+}$,$Na^{+}$ phosphors, and the inset is a zoom-in picture of a single particle; and (g–i) the corresponding EDS mapping of Ca, Sc, Si, Na and O, respectively.

 

remains an on-going issue due to the presence of impurity phases, which would degrade the luminescence performance. In this study, $Na^+$ ions are additionally introduced into the CSS host and serve as a charge compensator, which was found to effectively eliminate the impurity phase. The XRD patterns of CSS phosphors without and with $Na^+$ doping are shown in Fig. 1a. The XRD patterns of both phosphors are in agreement with the standard card of $Ca_3Sc_2Si_3O_{12}$ (ICSS No 72-1969). Impurity phases of $Sc_2O_3$ and $CeO_2$ always appear in the absence of $Na^+$ and they disappear when codoping with $Na^+$. In the CSS host trivalent $Ce^{3+}$ is expected to substitute for divalent $Ca^{2+}$ (a dodecahedral site),[34] leaving an effective positive charge around the local site, leading to some structural disorder and lattice defects around $Ce^{3+}$ due to the charge mismatch. For $Na^+$ ions in the CSS host, due to the similar ionic radius, they prefer to occupy $Ca^{2+}$ sites with an effective negative charge therein. The charge imbalance is greatly weakened, which then contributes to enhance the solubility of $Ce^{3+}$ in the CSS phosphors while eliminating the impurity phase.

Fig. 1b depicts the PL and PLE spectra of CSS:$Ce^{3+}$,$Na^+$ phosphors. The PLE spectrum shows a broad excitation peak at 445 nm, which is attributed to the absorption of the allowed transition from 4f to $5d_1$ of $Ce^{3+}$. This makes the CSS:$Ce^{3+}$,$Na^+$ phosphors to be effectively excited by commercial blue LED/LD chips. The PL spectrum ($\lambda_{ex}$ = 445 nm) exhibits a broad and strong cyan emission band with a peak at 508 nm and a FWHM of ~109 nm. Compared with the $Ce^{3+}$ emission peaking at 530 nm in LuAG, CSS:$Ce^{3+}$,$Na^+$ phosphors are expected to fill the aforementioned "Cyan cavity" and achieve extra-high color rendering because their PL intensity at 490 nm still remains at 70% of that at 508 nm (Fig. S1, ESI†). The asymmetric emission band can be decomposed into two Gaussian bands centered at 19 920 $cm^{-1}$ (*ca.* 502 nm) and 18 414 $cm^{-1}$ (*ca.* 543 nm) with an energy difference of 1506 $cm^{-1}$, which derive from the transitions of $Ce^{3+}$ from the 5d excited state to the $^2F_{5/2}$ and $^2F_{7/2}$ ground state (Fig. S1, ESI†). Furthermore, with the codoping of $Na^+$, the emission spectrum exhibits a slight red shift of ~3 nm from 505 nm to 508 nm, which was caused mainly by the increase of $Ce^{3+}$ concentration.[39] The CSS:$Ce^{3+}$,$Na^+$ phosphors are light green under daylight and exhibit bright green emission when exposed to UV lamp irradiation (the inset in Fig. 1b).

The PL performance of CSS:$Ce^{3+}$,$Na^+$ phosphors can be evaluated in terms of AE, IQE and EQE, as shown in Fig. 1c. By the introduction of $Na^+$ into phosphors, the IQE value was improved from 75% to as high as 85% due to the reduced crystal defects. The AE value also increased from 55% to 63% because of the increased $Ce^{3+}$ concentration incorporated in the CSS host. Moreover, the enhanced crystallinity of phosphors also plays an important role in increasing the IQE. Thus, highly efficient CSS:$Ce^{3+}$,$Na^+$ cyan-green phosphors with an EQE (54%) comparable to that of commercial green LuAG:$Ce^{3+}$ phosphors (with IQE, AE and EQE values of 97%, 58% and 56%, respectively) were obtained. SEM images in Fig. 1d display that the phosphors have an irregular shape and their particle size ranges from 7 to 15 μm. Fig. 1e shows the fluorescence microscope picture of CSS:$Ce^{3+}$,$Na^+$ phosphors in which the phosphors emit bright green light under blue light excitation. The EDS elemental mapping (Fig. 1f–k) of a selected CSS:$Ce^{3+}$,$Na^+$ particle shows the uniform distribution of Ca, Sc, Si and Na elements in phosphors, providing further evidence that the dopant $Na^+$ ions have been incorporated into the CSS host lattice.

### 3.2 Fabrication and microstructure of the CSS-PiG film

To demonstrate their potential in high-power laser lighting, the CSS-PiG films were fabricated by cofiring the mixture of glass powders and CSS:$Ce^{3+}$,$Na^+$ phosphors on a high-thermal-conductivity sapphire substrate. The schematic illustration of the preparation process is shown in Fig. 2. A low-melting-temperature borosilicate glass with the composition $26B_2O_3$-$35ZnO$-$12SiO_2$-$10La_2O_3$-$11WO_3$-$6Li_2O$ (in mol%) was chosen as an inorganic adhesive.[40] The glass was designed to match its refractive index ($n$ ~ 1.77, Fig. S2, ESI†) with that of CSS phosphors ($n$ ~ 1.78),[41] which favors to relieve the adverse light scattering and thus improve the luminescence efficiency of PiG films. Moreover, the glass matrix has a similar expansion coefficient to that of sapphire, which can eliminate the cracking and delamination of the PiG film.[40]

In order to achieve the outstanding performance of the CSS-PiG films, the sintering temperature and holding time were carefully controlled. These two key sintering parameters were optimized by examining the AE, IQE and EQE values of the PiG films under 445 nm excitation (Fig. 3). It can be seen that the IQE of the film increases with increasing sintering temperature. When the sintering temperature increases up to 700 °C, the IQE increases by ~10% and reaches as high as 92%. Both IQE and AE values are obviously improved when the sintering temperature increases from 600 to 640 °C. However, the AE value starts to decrease gradually as the sintering temperature further increases. Higher sintering temperature does not benefit the AE of the PiG film due to the decreased transmittance of the glass matrix (Fig. S3, ESI†). When considering the EQE, the optimal sintering temperature is 640 °C. Similarity, the holding time is optimized to be 40 min.

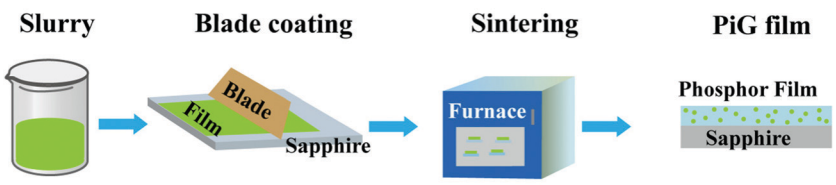


Fig. 2 Fabrication schematic of the PiG film.

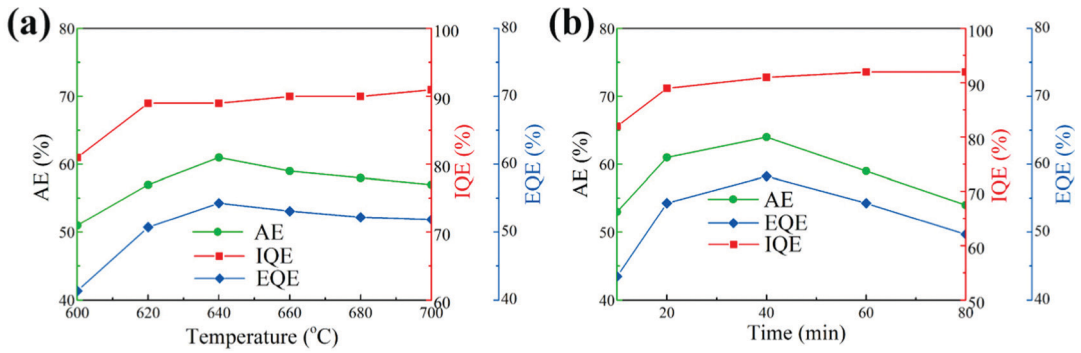


Fig. 3 Variations of the IQE, EQE and AE of CSS-PiG samples (P2G3, 73 μm) fired (a) at different temperatures for 20 min, and (b) at 640 °C for varying holding times.

The maximum transmittance of the blank glass film and PiG film (P2G3, 73 μm) sintered at 640 °C for 40 min can achieve 77% and 48% in the whole region above 500 nm (Fig. S3 and S4, ESI†). Thus, 640 °C and 40 min are the optimal sintering temperature and holding time.

Interestingly, the IQE of the PiG film is higher than that of its raw phosphors, which was found to be commonly decreased after the additional sintering into the PiG film.[42,43] This improvement is probably caused by the mild interface reactions between the phosphor surface and the glass matrix, which contributes to minimize the surface defects. In our experiments, CSS phosphors, prepared by the solid-state reaction, were fully ground to achieve micron size particles. Many surface defects or traps are produced from this pulverization process, which can quench the luminescence in the phosphor particles.[44] On the other hand, the mild interface reaction between the phosphor surface and the glass matrix would minimize the surface defects and improve the IQE of the PiG film. In addition, the good refractive index matching between the glass matrix and the CSS phosphor also contributes to improve the IQE of the PiG film. The maximal IQE and EQE of the PiG film (P2G3, 73 μm) are 89% and 57%, respectively.

The top view image of the CSS-PiG films showed that the CSS phosphors were well-wetted and adequately embedded in the glass matrix (Fig. 4a). Due to the viscous flow of the glass matrix during the sintering process, the PiG film is characterized by a relatively flat surface and a fully dense structure. The words under the PiG film can be observed clearly, which indicates the

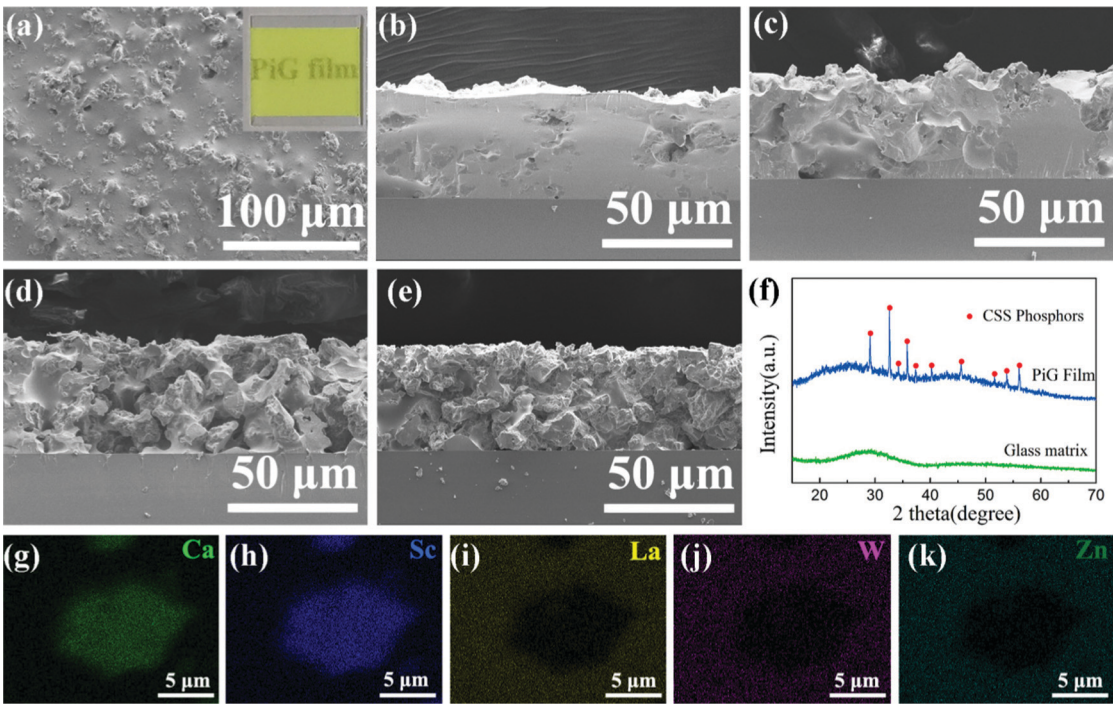


Fig. 4 (a) Top view image of the P2G3 film (50 μm) and the inset is the photograph of the film; (b–e) cross-sectional SEM images of PiG films with different PiG ratios at a fixed thickness of ~50 μm (P1G4, P2G3, P3G2 and P4G1, respectively); (f) XRD patterns of the glass powders and the PiG film (P2G3, 73 μm); and (g–k) EDS mappings of the P1G4 film.

 

dense structure of the film. Fig. 4b–e are the cross-sectional SEM images of PiG films with different PiG ratios (P1G4, P2G3, P3G2 and P4G1, respectively) at a fixed thickness of ~50 μm. It is found that all PiG films are tightly bonded to the sapphire substrate. The phosphor particles are uniformly dispersed in the glass matrix and residual pores are difficult to observe in the P1G4 film. With the increase of the phosphor content, more pores are observed in the PiG film because the reduced glass content makes it difficult to remove the trapped holes during the sintering process. As a result, the total transmittance of the PiG film decreases dramatically at higher phosphor content (Fig. S4a, ESI†). For the same PiG ratio, the total transmittance also decreased with the increase of the thickness (Fig. S4b, ESI†). The XRD patterns of the CSS-PiG film (P2G3, 73 μm) present obvious diffraction peaks belonging to the CSS phosphors and an amorphous hump from the glass matrix (Fig. 4f). No phase transition occurs during the sintering process. It can also be confirmed by the clear boundary between the CSS phosphors and the glass matrix, as shown in Fig. 4g–k.

### 3.3 Photoluminous and thermal stability of the CSS-PiG film

As shown in Fig. 5a, the PLE and PL spectra of the PiG film are similar to those of the corresponding CSS:$Ce^{3+}$,$Na^{+}$ phosphors. However, due to the absorption of the glass matrix in the ultraviolet range, the 310 nm excitation band of the PiG film is much lower than that of phosphors, while the blue excitation is not significantly affected by the surrounding glass matrix. The decay curves of the phosphors and PiG are shown in Fig. 5b. The lifetimes of the CSS-PiG film and the phosphors were calculated to be 72.8 ns and 69.6 ns, respectively. They almost have the same decays. The thermal stability of the phosphor converter is a critical parameter for high-power density laser lighting, which determines the reliability and efficiency of the whole device. Fig. 5c presents the temperature-dependent normalized PL intensity of the PiG film under 0.2 W blue laser excitation. For the CSS-PiG film, the integrated PL intensity exhibits quite a linear decrease upon increasing the temperature from 25 to 300 °C. For the YAG-PiG film, the intensity shows a slight decline between 25 and 175 °C, followed by a dramatic decrease at higher temperature. In comparison with the YAG-PiG film, the CSS-PiG film exhibits much better thermal stability especially at temperature higher than 200 °C, in agreement with the previous reports.[45] The emission intensity of the CSS-PiG film drops to 89.5% of the initial intensity when the temperature rises from 25 to 200 °C and remains at 75% at 300 °C. In contrast, the commercial YAG:Ce maintains only 62% at 300 °C. The excellent thermal stability of the CSS-PiG film suggests its promising potential for application in efficient high-power-density laser lighting, which commonly requires high thermal stability of luminescence at least up to 200 °C.[30,46] It should be noted that the thermal stability of CSS-PiG is comparable to that of the corresponding phosphors. The unimpaired luminescence properties of the PiG film imply that the intactness of CSS:$Ce^{3+}$,$Na^{+}$ phosphors is well preserved during the sintering process.

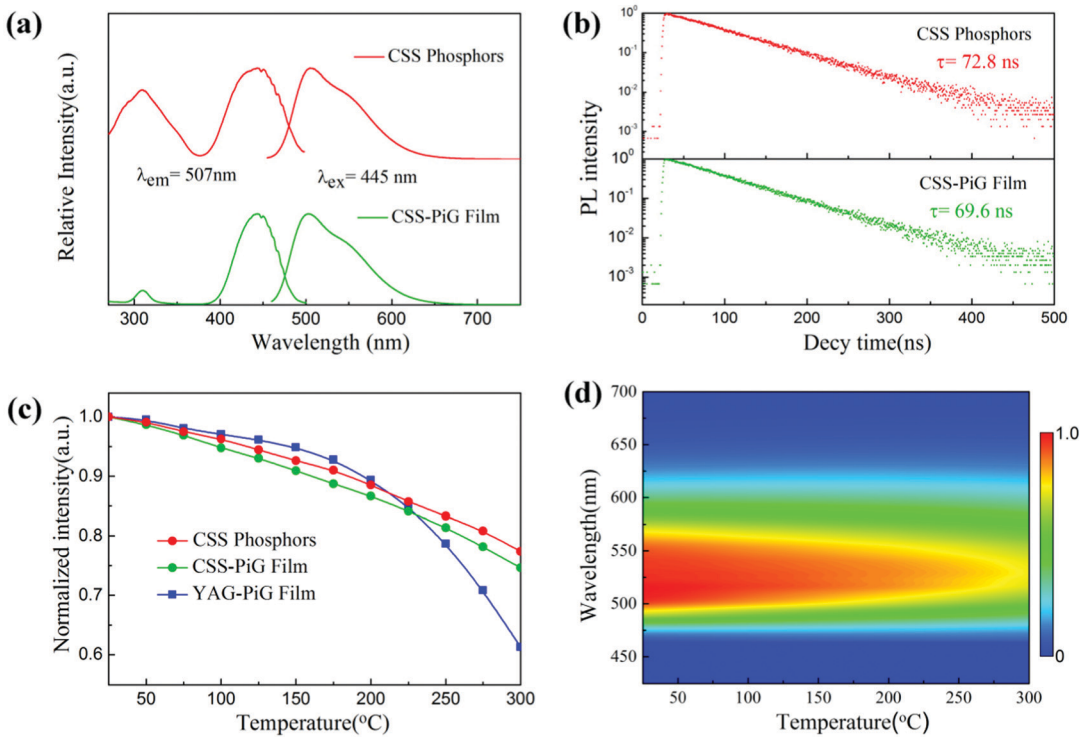


Fig. 5 Normalized PL and PLE spectra (a) and decay curves (b) of the CSS:$Ce^{3+}$,$Na^{+}$ phosphors and the CSS-PiG film (P2G3, 73 μm); temperature-dependent integrated emission intensity (c) and the corresponding emission spectra of the CSS-PiG film (d). The measuring temperature was varied from 25 to 300 °C.

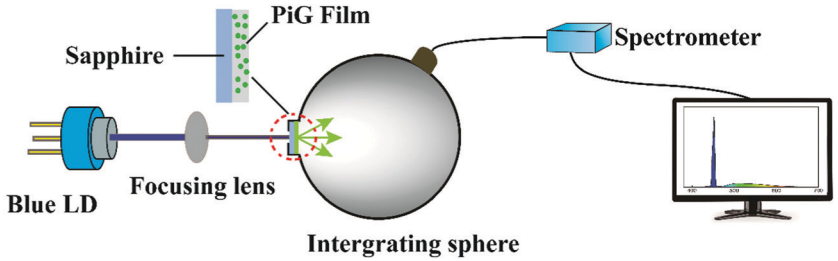


Fig. 6 Schematic illustration of measuring the laser lighting performance of the PiG film in a transmissive configuration.

### 3.4 Optical properties of the CSS-PiG film under blue laser excitation

The performance of the CSS-PiG films in laser lighting was evaluated under blue laser excitation. The measurement was conducted in a transmissive configuration equipped with a 452 nm blue laser, as illustrated in Fig. 6. To determine the optimized phosphor content, PiG films with different PiG ratios were investigated at a fixed thickness of ~73 μm under a 0.97 W blue laser. As the PiG ratio increases, the transmitted blue light decreases significantly because of the enhanced blue absorption, whereas the forward converted cyan-green light reaches its maximum at the PiG ratio of 2:3 (Fig. 7b). With the further increase of the phosphor content, the forward cyan-green light decreases slowly due to the increased backscattering loss. The forward optical-to-optical conversion efficiency, defined as the ratio of the forward converted cyan-green light power to the reduced blue light power (*i.e.*, the difference between the incident blue laser power and the transmitted blue light power), is shown in Fig. 7b. It reaches a maximum of 43% at the PiG ratio of 2:3. The corresponding CIE color coordinates of the constructed white laser lighting change from blue to white and finally to green, which are in accordance with their luminescence images (the insets in Fig. 7c). Therefore, the optimized PiG ratio of P2G3 results in both high light conversion efficiency and satisfied CIE color coordinates. In addition, the thickness-dependent optical properties of the PiG films were also investigated with a fixed PiG ratio of 2:3. The transmitted blue light exhibits a monotonous decrement with its increasing thickness, and the color coordinates correspondingly shift from blue to white and finally to green (Fig. 7d). The forward cyan-green light reaches its maximum at a thickness of 95 μm. Upon considering the forward conversion efficiency and color coordinates, the film with a PiG ratio of 2:3 and a thickness of 73 μm shows the superior performance for laser lighting.

The luminescence properties of the optimized film (P2G3, 73 μm) in laser lighting were detailed by varying the incident blue laser power. On increasing the incident laser power from 0.52 to 6.24 W, the emission intensity of the film increases monotonously (Fig. 8a). But when the laser power increases to 6.61 W, luminous saturation is observed and the emission intensity of the film drops sharply. The increase of emission

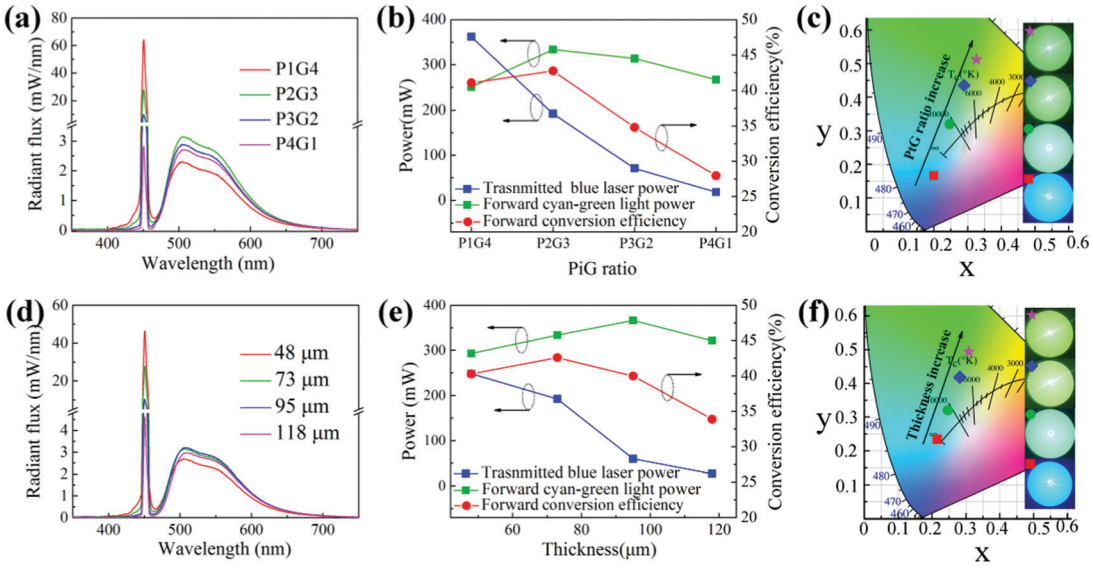


Fig. 7 EL spectra (a), transmitted blue laser power, forward converted cyan-green light power, and the forward optical to optical conversion efficiency (b) and the corresponding CIE color coordinates (c) of the film with different PiG ratios (~73 μm); EL spectra (d), transmitted blue laser power, forward converted cyan-green light power, and the forward light conversion efficiency (e) and the corresponding CIE color coordinates (f) of the film with varying film thickness (P2G3). The insets are the corresponding luminescence images.

 

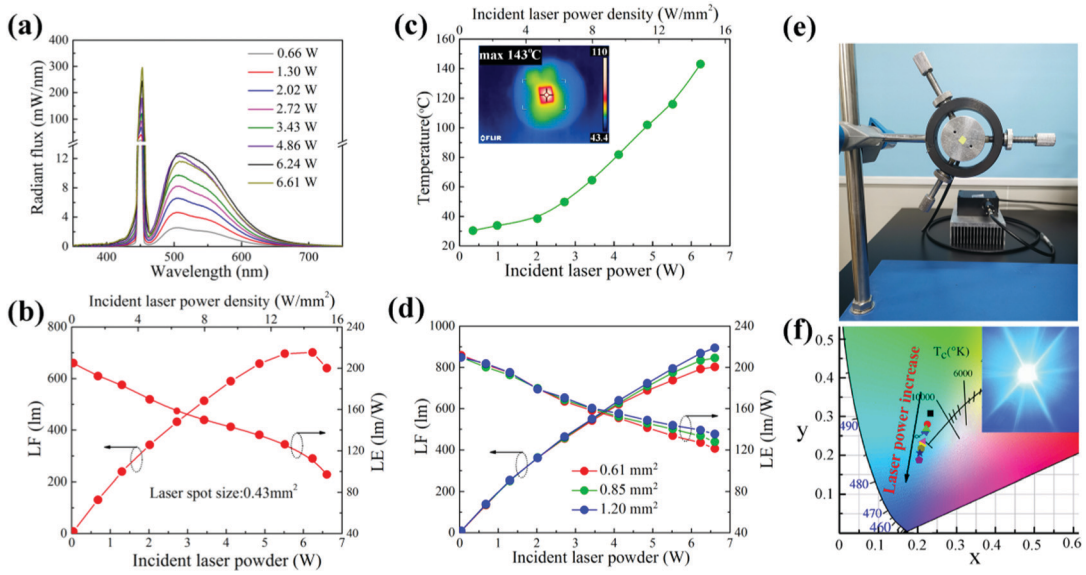


Fig. 8 EL spectra (a), LF and LE (b), and surface temperature (c) of the CSS-PiG film (P2G3, 73 μm) pumped by varying blue laser power with a laser spot size of 0.43 $mm^2$; (d) LF and LE of the film excited with varying laser spot size; (e) photograph of the laser lighting device with blue LD off; and (f) the CIE color coordinate of the film excited by varying blue laser power (0.43 $mm^2$). The inset of (c) is the thermal infrared image of the CSS film under the 6.24 W blue laser excitation and the inset of (f) is the corresponding lighting image.

intensity arises from the increased absorption and photon conversion of the blue light to cyan-green light by $Ce^{3+}$ ions. The sudden decrease in luminous flux can be attributed to the severe thermal quenching due to the dramatically elevated temperature under high-density laser excitation. When the incident laser power is higher than a threshold value, the heat cannot be efficiently dissipated but accumulates and increases the temperature of the sample continuously. The high temperature would quench the luminescence by transforming the excitation light energy into phonons. The luminous saturation would accordingly occur and the forward luminous efficacy (LE) would drop sharply. The maximum forward luminous flux (LF) reaches 701 lm at an incident laser power of 6.24 W and the corresponding laser power density is 14.5 W $mm^{-2}$ (Fig. 8b). As shown in Fig. 8c, the laser spot temperature of the film attached to a polished pure aluminum block was measured by an infrared thermal image. With the increase of the incident laser power, the peak temperature of the laser spot increases dramatically. At a laser power of 6.24 W, the temperature reaches an equilibrium temperature as high as 143 °C in 40 seconds (Fig. 8c and Fig. S5, ESI†). The emission band shows a red shift due to the thermal effect, which is similar to that observed in Fig. 3 (Fig. S6, ESI†). On the other hand, the CIE color coordinates move towards the blue region due to the increased transmittance of blue light and the declined conversion efficiency at elevated temperature (Fig. 8f). The inset in Fig. 8f shows intense cyan emission, due to the mixing of the cyan-green emission with transmitted blue light. Moreover, when pumped by a blue laser with larger laser spot size, luminescence saturation does not occur and the luminous efficacy is also improved due to the reduced thermal quenching (Fig. 8d). Thus, the laser spot size in laser lighting should be carefully controlled to balance the brightness and LE.

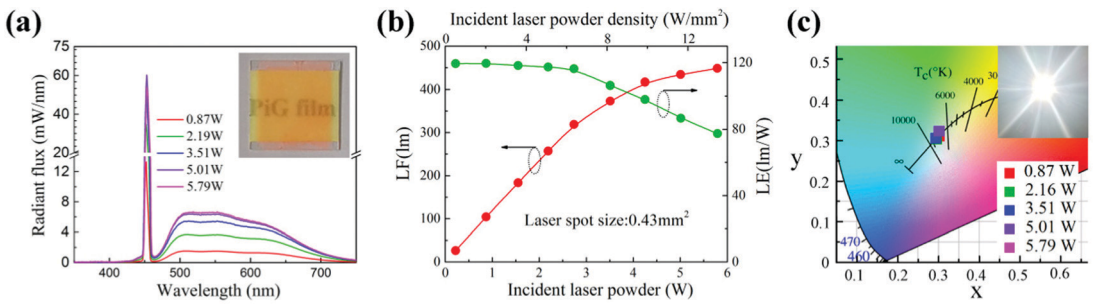


Fig. 9 (a) EL spectra, (b) LF and LE and (c) the corresponding CIE color coordinate of the composite film (CSS-PiG/$CaAlSiN_3$) driven by varying blue laser power. The inset of (a) is the photograph of the composite film; the inset of (c) is the lighting image of the composite film under the excitation of a 5.79 W blue laser.

Table 1 LF, LE, CRI, CCT, and chromaticity coordinates ($x$, $y$) of the composite film driven by different laser power

| Laser power (W) | Power density (W mm$^{-2}$) | LF (lm) | LE (lm W$^{-1}$) | CIE-$x$ | CIE-$y$ | $R_a$ | CCT (K) |
|---|---|---|---|---|---|---|---|
| 0.87 | 2.0 | 104 | 120 | 0.307 | 0.319 | 93 | 6937 |
| 2.19 | 5.2 | 257 | 117 | 0.302 | 0.311 | 93 | 7357 |
| 3.51 | 8.2 | 373 | 106 | 0.296 | 0.304 | 93 | 7944 |
| 5.01 | 11.7 | 434 | 86 | 0.294 | 0.306 | 92 | 8082 |
| 5.79 | 13.5 | 448 | 77 | 0.302 | 0.323 | 91 | 7203 |

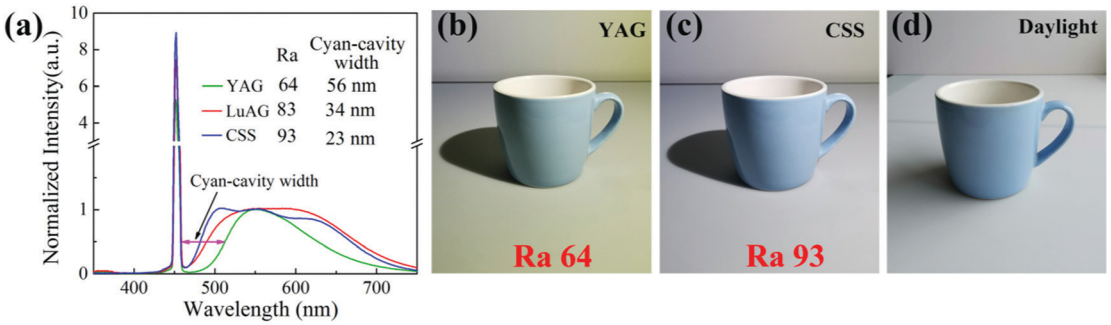


Fig. 10 (a) Normalized EL spectra of the white laser light encapsulated with the YAG-PiG film, LuAG/$CaAlSiN_3$-PiG film and CSS-PiG/$CAlSiN_3$ film; and (b–d) photographs of a cyan cup under different laser light or daylight.

### 3.5 Optical properties of the composite PiG film under blue laser excitation

Although the CSS-PiG film exhibits excellent thermal stability and high LE, the CRI of this phosphor converted white light is low (~61) due to the deficiency of the red component. A composite film was designed by coating the red-emitting layer of $CaAlSiN_3$-PiS on the CSS-PiG film to improve the color rendering of white laser lighting. Fig. 9 and Table 1 present the optical performance of the composite CSS-PiG/$CAlSiN_3$ film. Overall, the composite film shows an ultra-broadband emission from 470 to 750 nm with a FWHM of ~196 nm. With increasing laser power from 0.88 to 5.79 W, the emission intensity of the sample increases monotonously (Fig. 9a). The LE decreases at the higher incident laser power; however, the CIE chromaticity coordinates almost remain constant, indicating the super chromaticity stability of the composite film. As shown in Table 1, the sample yields a uniform white light with a maximum LF of 448 lm, a LE of 78 lm W$^{-1}$, chromaticity coordinates of (0.3018, 0.3227) and an $R_a$ of 91 under 5.79 W blue laser excitation (13.5 W mm$^{-2}$). In comparison with the CSS-PiG film, the composite film shows much higher color rendering at the expense of a relatively lower LE. As shown in Fig. S7 (ESI†), there is a big spectral overlap between the emission spectrum of CSS:$Ce^{3+}$ and the excitation spectrum of $CaAlSiN_3$:$Eu^{2+}$. Therefore, much of the converted cyan-green light from the PiG film undergoes reabsorption loss when passing through the $CaAlSiN_3$ layer. Thus, there is a large space to optimize the optical performance of the composite film for laser lighting. For example, we can select more suitable red phosphors, which can avoid the reabsorption effect. In addition, the LE of the CSS-PiG film can also be improved through coating a blue-pass filter and an antireflection layer on the sapphire, which would improve the blue transmittance and simultaneously hold back the backward emission of the phosphors.[30] But anyhow, the CSS-PiG film is a promising candidate for high-power laser-driven white lighting.

The luminescence performance of the white laser light encapsulated with the YAG-PiG film, LuAG/$CaAlSiN_3$-PiG film and CSS-PiG/$CAlSiN_3$ film is shown in Fig. 10. The "Cyan cavity" between the incident blue laser and the converted emission peak was measured by the FWHM of the cavity, as shown in Fig. 10a. Compared with other films, the CSS-PiG/$CAlSiN_3$ film has a much wider emission spectrum, which remarkably narrows the "Cyan cavity" and thus provides a $R_a$ above 90 (Fig. 10a). The photographs of a cyan cup taken under different light are shown in Fig. 10b. There is an obvious discrepancy among them. The cup is light cyan under laser light with a $R_a$ of 64, while it is bright cyan under laser light with higher $R_a$. These results confirm that the composite CSS-PiG/$CAlSiN_3$ film offers great potential for application in laser lighting with excellent color rendering.

## 4. Conclusion

In summary, phase-pure CSS:$Ce^{3+}$,$Na^+$ phosphors with high IQE (85%) were developed by introducing charge compensatory additive $Na^+$ into the CSS lattice. A CSS-PiG film was further prepared by cofiring the CSS:$Ce^{3+}$,$Na^+$ phosphors and glass powders on a sapphire substrate, providing cyan emission peaking at 508 nm. After the optimized co-firing process (640 °C, 40 min), the IQE of the film was further improved to 91%. Moreover, the PiG film exhibits excellent thermal stability with an integrated emission of 75% even at 300 °C. By optimizing the phosphor content and film thickness (P2G3, 73 μm), a

 

maximum forward optical-to-optical conversion efficiency of 43% was obtained for the PiG film. Under the 14.5 W $mm^{-2}$ blue laser excitation, the film yields a white light with a LF of 701 lm, a LE of 112 lm $W^{-1}$ and a $R_a$ of 61. A higher $R_a$ of 93 was obtained by further coating the red $CaAlSiN_3$ layer onto the CSS-PiG film. These results make the composite film a promising candidate for high-brightness laser-driven white lighting with excellent color rendering.

## Conflicts of interest

There are no conflicts to declare.

## Acknowledgements

This work was partially supported by the National Natural Science Foundation of China (Grant No. 51772286, 11874055, 11974346, 11904361, 12074373, 12074374 and 52072361), Youth Innovation Promotion Association CAS No. 2020222, Key Research and Development Program of Jilin province (20200401050GX), Cooperation project between Jilin Province and Chinese Academy of Sciences (2020SYHZ0013).

## References

1 J. H. Oh, S. J. Yang and Y. R. Do, *Light: Sci. Appl.*, 2014, **3**, e141.
2 J. J. Wierer, J. Y. Tsao and D. S. Sizov, *Laser Photonics Rev.*, 2013, **7**, 963–993.
3 S. H. Lim, Y. H. Ko, C. Rodriguez, S. H. Gong and Y. H. Cho, *Light: Sci. Appl.*, 2016, **5**, e16030.
4 X. Qin, X. W. Liu, W. Huang, M. Bettinelli and X. G. Liu, *Chem. Rev.*, 2017, **117**, 4488–4527.
5 Z. Xia and A. Meijerink, *Chem. Soc. Rev.*, 2017, **46**, 275–299.
6 Y. H. Wang, J. Y. Ding, Y. C. Wang, X. F. Zhou, Y. X. Cao, B. Ma, J. Y. Li, X. C. Wang, T. Seto and Z. Y. Zhao, *J. Mater. Chem. C*, 2019, **7**, 1792–1820.
7 L. Wang, R. J. Xie, T. Suehiro, T. Takeda and N. Hirosaki, *Chem. Rev.*, 2018, **118**, 1951–2009.
8 X. F. Li, J. D. Budai, F. Liu, J. Y. Howe, J. H. Zhang, X. J. Wang, Z. J. Gu, C. J. Sun, R. S. Meltzer and Z. W. Pan, *Light: Sci. Appl.*, 2013, **2**, e50.
9 Z. W. Jia, C. X. Yuan, Y. F. Liu, X. J. Wang, P. Sun, L. Wang, H. C. Jiang and J. Jiang, *Light: Sci. Appl.*, 2020, **9**, 86.
10 J. J. Wierer and J. Y. Tsao, *Phys. Status Solidi A*, 2015, **212**, 980–985.
11 H. Lin, T. Hu, Y. Cheng, M. Chen and Y. Wang, *Laser Photonics Rev.*, 2018, **10**, 56.
12 S. X. Li, L. Wang, N. Hirosaki and R. J. Xie, *Laser Photonics Rev.*, 2018, **12**, 1800173.
13 Y. H. Kim, N. S. M. Viswanath, S. Unithrattil, H. J. Kim and W. B. Im, *ECS J. Solid State Sci. Technol.*, 2017, **7**, R3134–R3147.
14 T. W. Kang, K. W. Park, J. H. Ryu, S. G. Lim, Y. M. Yu and J. S. Kim, *J. Lumin.*, 2017, **191**, 35–39.
15 Q. Sai, Z. Zhao, C. Xia, X. Xu, F. Wu, J. Di and L. Wang, *Opt. Mater.*, 2013, **35**, 2155–2159.
16 W. Nian, L. Tiecheng, L. Feng, Z. Wei, M. Benyuan, L. Zhongwen and Q. Jianqi, *Appl. Phys. Lett.*, 2012, **101**, 061902.
17 Y. Liu, S. Liu, P. Sun, Y. Du, S. Lin, R. J. Xie, R. Dong, J. Jiang and H. Jiang, *ACS Appl. Mater. Interfaces*, 2019, **11**, 21697–21701.
18 Q. Yao, P. Hu, P. Sun, M. Liu, R. Dong, K. F. Chao, Y. F. Liu, J. Jiang and H. C. Jiang, *Adv. Mater.*, 2019, **32**, 1907888.
19 C. Cozzan, G. Lheureux, N. O'Dea, E. E. Levin, J. Graser, T. D. Sparks, S. Nakamura, S. P. DenBaars, C. Weisbuch and R. Seshadri, *ACS Appl. Mater. Interfaces*, 2018, **10**, 5673–5681.
20 D. Zhang, W. G. Xiao, C. Liu, X. F. Liu, J. J. Ren, B. B. Xu and J. R. Qiu, *Nat. Commun.*, 2020, **11**, 2805.
21 X. Zhang, J. Yu, J. Wang, B. Lei, Y. Liu, Y. Cho, R.-J. Xie, H.-W. Zhang, Y. Li, Z. Tian, Y. Li and Q. Su, *ACS Photonics*, 2017, **4**, 986–995.
22 R. Zhang, H. Lin, Y. Yu, D. Chen, J. Xu and Y. Wang, *Laser Photonics Rev.*, 2014, **8**, 158–164.
23 Y. J. Park, S. W. Kim, C. J. Kim, Y. J. Lee and J. Hwang, *J. Alloys Compd.*, 2019, **794**, 94–100.
24 T. Hu, L. X. Ning, Y. Gao, J. W. Qiao, E. H. Song, Z. T. Chen, Y. Y. Zhou, J. Wang, M. S. Molokeev, X. X. Ke, Z. G. Xia and Q. Y. Zhang, *Light: Sci. Appl.*, 2021, **10**, 12.
25 J. Park, J. Kim and H. Kwon, *Adv. Opt. Mater.*, 2017, **5**, 1700347.
26 S. H. You, S. X. Li, P. Zheng, T. L. Zhou, L. Wang, L. H. Liu, N. Horisaki, F. F. Xu and R. J. Xie, *Laser Photonics Rev.*, 2019, **13**, 1800216.
27 J. Xu, Y. Yang, Z. Q. Guo, B. F. Hu, J. Wang, B. L. Du, B. G. Liu, H. P. Ji, C. Dam-Hansen and O. B. Jensen, *J. Eur. Ceram. Soc.*, 2020, **40**, 4704–4708.
28 H. Wu, Z. Hao, G.-H. Pan, L. Zhang, H. Wu, X. Zhang, L. Zhang and J. Zhang, *J. Eur. Ceram. Soc.*, 2020, **40**, 2439–2444.
29 X. J. Zhang, S. C. Si, J. B. Yu, Z. J. Wang, R. H. Zhang, B. F. Lei, Y. L. Liu, J. L. Zhuang, C. F. Hu, Y. J. Cho, R. J. Xie, H. W. Zhang, Z. F. Tian and J. Wang, *J. Mater. Chem. C*, 2019, **7**, 354–361.
30 P. Zheng, S. Li, L. Wang, T. L. Zhou, S. You, T. Takeda, N. Hirosaki and R. J. Xie, *ACS Appl. Mater. Interfaces*, 2018, **10**, 14930–14940.
31 M. Zhao, H. X. Liao, M. S. Molokeev, Y. Y. Zhou, Q. Y. Zhang, Q. L. Liu and Z. G. Xia, *Light: Sci. Appl.*, 2019, **8**, 38.
32 R. Xiang, X. Liang, P. Li, X. Di and W. Xiang, *Chem. Eng. J.*, 2016, **306**, 858–865.
33 L. Wang, R. Wei, P. Zheng, S. You, T. Zhou, W. Yi, T. Takeda, N. Hirosaki and R.-J. Xie, *J. Mater. Chem. C*, 2020, **8**, 1746–1754.
34 Y. Shimomura, T. Honma, M. Shigeiwa, T. Akai, K. Okamoto and N. Kijima, *J. Electrochem. Soc.*, 2007, **154**, J35.
35 Y. Liu, X. Zhang, Z. Hao, Y. Luo, X. Wang and J. Zhang, *J. Lumin.*, 2012, **132**, 1257–1260.
36 Y. F. Wu, Y. H. Chan, Y. T. Nien and I. G. Chen, *J. Am. Ceram. Soc.*, 2013, **96**, 234–240.
37 F. J. Pan, M. Zhou, J. H. Zhang, X. J. Zhang, J. Wang, L. Huang, X. J. Kuang and M. M. Wu, *J. Mater. Chem. C*, 2016, **4**, 5671–5678.
38 Z. Jia, C. Yuan, Y. Liu, X.-J. Wang, P. Sun, L. Wang, H. Jiang and J. Jiang, *Light: Sci. Appl.*, 2020, **9**, 86.

39 Y. Shimomura, T. Kurushima, M. Shigeiwa and N. Kijima, *J. Electrochem. Soc.*, 2008, **155**, J45.
40 Y. Peng, Y. Mou, Q. Sun, H. Cheng, M. Chen and X. Luo, *J. Alloys Compd.*, 2019, **790**, 744–749.
41 M. Mikami, H. Watanabe, K. Uheda, S. Shimooka, Y. Shimomura, T. Kurushima and N. Kijima, *IOP Conf. Ser.: Mater. Sci. Eng.*, 2009, **1**, 012002.
42 S. You, S. Li, L. Wang, T. Takeda, N. Hirosaki and R.-J. Xie, *Chem. Eng. J.*, 2020, **404**, 126575.
43 B. Wang, H. Lin, J. Xu, H. Chen and Y. Wang, *ACS Appl. Mater. Interfaces*, 2014, **6**, 22905–22913.
44 Z. He, W. Cheng, Z. Li, Y. Liu, Q. Ou and R. Liang, *J. Lumin.*, 2013, **136**, 351–354.
45 S. K. Sharma, Y.-C. Lin, I. Carrasco, T. Tingberg, M. Bettinelli and M. Karlsson, *J. Mater. Chem. C*, 2018, **6**, 8923–8933.
46 J. Wang, X. Tang, P. Zheng, S. Li, T. Zhou and R.-J. Xie, *J. Mater. Chem. C*, 2019, **7**, 3901–3908.

 